Impact of stoichiometry and disorder on the electronic structure of the PbBi$_2$Te$_{4-x}$Se$_x$ topological insulator

I. A. Shvets,[1,2] I. I. Klimovskikh,[2] Z. S. Aliev,[3,4] M. B. Babanly,[5] J. Sánchez-Barriga,[6]
M. Krivenkov,[6] A. M. Shikin,[2] and E. V. Chulkov[7,8,1,2]

[1]*Tomsk State University, Tomsk 634050, Russia*
[2]*St. Petersburg State University, Saint Petersburg 198504, Russia*
[3]*Azerbaijan State Oil and Industry University, AZ1010 Baku, Azerbaijan*
[4]*Institute of Physics, ANAS, AZ1143 Baku, Azerbaijan*
[5]*Institute of Catalysis and Inorganic Chemistry, ANAS, AZ1143 Baku, Azerbaijan*
[6]*Helmholtz-Zentrum Berlin für Materialien und Energie, Elektronenspeicherring BESSY II,*
Albert-Einstein-Strasse 15, 12489 Berlin, Germany
[7]*Donostia International Physics Center (DIPC), 20018 San Sebastián/Donostia, Basque Country, Spain*
[8]*Departamento de Física de Materiales UPV/EHU, Centro de Física de Materiales CFM - MPC and Centro Mixto CSIC-UPV/EHU,*
20080 San Sebastián/Donostia, Basque Country, Spain

Detailed comparative theoretical and experimental study of electronic properties and spin structure was carried out for a series of Pb-based quaternary compounds PbBi$_2$Te$_{4-x}$Se$_x$. For all values of x, these compounds are theoretically predicted to be topological insulators, possessing at high Se content a remarkably large band gap and a Dirac point isolated from bulk states. Using spin- and angle-resolved photoemission spectroscopy, it was shown that the PbBi$_2$Te$_2$Se$_2$ and PbBi$_2$Te$_{1.4}$Se$_{2.6}$ compounds are characterized by well-defined spin-polarized topological surface state in the bulk gap. To define the probable distribution of atoms over the atomic sites for these samples, we performed *ab initio* calculations in ordered and disordered configurations of the unit cell. We found that theoretical calculations better reproduce photoemission data when Te atoms are placed in the outermost layers of the septuple layer block.

I. INTRODUCTION

One of the milestone ideas of spintronics is creation of spin current in nonmagnetic solids. The optimal electronic properties and spin structure for formation of this current is the Dirac-cone-like state with nondegenerate spin branches and opposite orientation of spin for opposite sign of wave vector. Such type of structure is found to be an essential characteristic of the surface electronic structure of topological insulators (TIs) [1,2]. To date, a large number of TIs have been discovered [1–9]. The most studied of them are compounds with tetradymite-like structure in which each atomic layer consists of only one sort of atoms. However, it is possible to obtain the disordered alloys with similar structure but with statistical distribution of different types of atoms [10–16]. In practice, the variation of the composition of multicomponent compounds allows for tuning the Fermi level to energy gap in materials where it is located in the bulk band, owing to the residual bulk charge induced by crystal defects [10–12,14–18].

As shown experimentally in Ref. [7], the fabrication of the Pb-based seven-layer PbBi$_2$Te$_4$ in the PbTe-Bi$_2$Te$_3$ system leads to the increase of the band gap from 165 meV [3] as for binary five-layer Bi$_2$Te$_3$ up to 230 meV and preserves properties inherent to TIs. Moreover, PbBi$_2$Te$_4$ is remarkable for the high surface charge carrier density [7]. On the other hand, for another binary compound, Bi$_2$Se$_3$, the gap is of 300 meV [4]. One would expect that this tendency of modification of the electronic structure by adding Pb atoms can be applied to Bi$_2$Se$_3$.

However, unlike PbTe-Bi$_2$Te$_3$ system in PbSe-Bi$_2$Se$_3$ alloys, grown in a bulk crystal form, the PbSe bilayers are not incorporated into five-layer slabs (Se-Bi-Se-Bi-Se) to form seven-layer slabs PbBi$_2$Se$_4$ containing Pb atoms in the central atomic plane (Se-Bi-Se-Pb-Se-Bi-Se) [19]. Instead, the chemical composition of PbSe-Bi$_2$Se$_3$ alloys can be expressed as [(PbSe)$_5$]$_n$[(Bi$_2$Se$_3$)$_3$]$_m$, according to which the crystal with monoclinic structure consists of m hexagonal quintuple layers of Bi$_2$Se$_3$ sandwiched by adjacent n bilayers of rock-salt PbSe [20], forming a natural multilayer heterostructure consisting of TI and an ordinary insulator. By means of angle-resolved photoemission spectroscopy for $n = 1$ it was shown that at $m = 2$ there is a gapped Dirac-cone state within the bulk band gap of 0.5 eV, while at $m = 1$ it disappears owing to no band inversion in the Bi$_2$Se$_3$ unit [21]. On the other hand, in the PbSe-PbTe-Bi$_2$Se$_3$-Bi$_2$Te$_3$ system for bulk crystals, the tetradymite phase extends from PbBi$_2$Te$_4$ up to PbBi$_2$Te$_{0.88}$Se$_{3.12}$, while at higher concentration of Se atoms the alloys exist in a monoclinic phase [22].

Nevertheless, a thin film of PbBi$_2$Se$_4$ with hexagonal structure was successfully grown [23] and on the base of the derived crystal parameters it was theoretically predicted [9,24] that this compound is supposed to be a very promising TI due to significantly large gap (up to 400 meV) and well-defined Dirac cone. Just recently, Chatterjee *et al.* [25] synthesized an ultrathin three- to five-septuple-layer PbBi$_2$Se$_4$ film that exhibits an n-type semiconducting behavior as well as a band gap of 600 meV.

Therefore, it is very instructive to study the influence of composition modification and atomic distribution on electronic structure of the alloy. Starting with PbBi$_2$Te$_4$, as it has been successfully grown and already well studied [7,26,27], by gradual substitution of tellurium by selenium one would
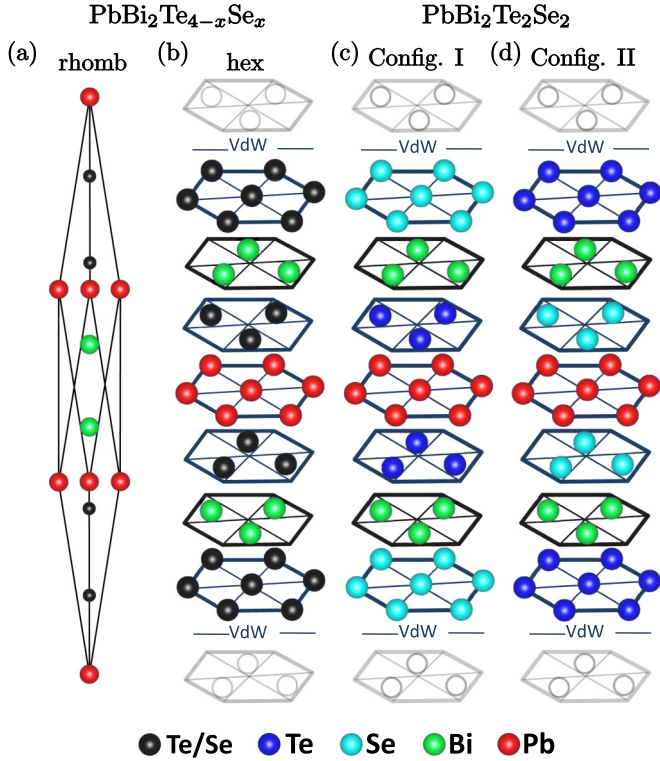
FIG. 1. Crystal structure in rhombohedral (a) and hexagonal (b) representations of the $PbBi_2Te_{4-x}Se_x$ compound. [(c), (d)] Crystal structure of the ordered $PbBi_2Te_2Se_2$ compound in its two possible configurations.

obtain the $PbBi_2Te_{4-x}Se_x$ alloy and in the limiting case ($x = 4$) approach $PbBi_2Se_4$. In the present work, we have performed a detailed comparative theoretical and experimental investigation of electronic and spin structure of series of the quaternary compounds $PbBi_2Te_{4-x}Se_x$ with fractional stoichiometry. For this purpose, we have synthesized samples of the intermediate composition ($x = 2.0$ and 2.6) and performed calculations in ordered and disordered configurations of the unit cell to define the probable distribution of atoms over the atomic sites. We have theoretically established that all compounds in this system are TIs and by means of spin- and angle-resolved photoemission spectroscopy (SARPES) observed a single Dirac-cone-like surface band structure in our grown samples.

II. EXPERIMENTAL AND COMPUTATIONAL DETAILS

$PbBi_2Te_{4-x}Se_x$ compounds have a rhombohedral centrosymmetric crystal structure [space group $R\bar{3}m$ (166)] with seven atoms in elementary cell [Fig. 1(a)], which can be represented in the hexagonal structure built of septuple layers (SL) with ionic-covalent bonds and separated by van der Waals spacings [Fig. 1(b)].

Crystal structure optimization and electronic band structure calculations were performed in the framework of relativistic density functional theory (DFT) using the ABINIT code [28]. In order to introduce the fractional ratio of concentration and simulate the disordering within atomic layers, a virtual crystal approximation (VCA) was applied, where the averaged

TABLE I. Experimental atomic parameters in hexagonal cell geometry for $PbBi_2Te_{4-x}Se_x$ at $x = 0, 1.92, 4$.

Compound	a (Å)	c (Å)
$PbBi_2Te_4$ [27]	4.439	41.677
$PbBi_2Te_{2.08}Se_{1.92}$ [22]	4.31	40.6
$PbBi_2Se_4$ [23]	4.16	39.2

pseudopotential of a "black" atom [Fig. 1(b)] occupying a site in the Te/Se sublattice is defined as a mixture $V_{VCA} = (4 - x)V_{Te} + xV_{Se}$ of Te (V_{Te}) and Se (V_{Se}) pseudopotentials. Here x accounts for relative concentration of the Te and Se atoms in the Te/Se layers and varies from 0 up to 4 with step of 0.5. We suppose that within the range of chosen x the alloy preserves one type of crystal structure. For each chosen x, the lattice constants were derived by linear interpolation of experimental values [22,23,27] in accordance with Vegard's law [29] (Table I).

To investigate the effect of disordering within the Te/Se sublattice on the bulk and surface electronic structure of $PbBi_2Te_2Se_2$ (and $PbBi_2Te_{1.4}Se_{2.6}$) compound, three possible cases of atomic structure were studied [see Figs. 1(b)–1(d)]. As for $PbBi_2Te_2Se_2$, they are the following: [Fig. 1(b)] Se and Te atoms are homogeneously mixed in all four layers within the SL block and [Fig. 1(c)] the outermost layers are occupied only by the Se atoms and, vice versa, [Fig. 1(d)] only by the Te atoms. The similar procedure was also done for $PbBi_2Te_{1.4}Se_{2.6}$. In this case, no ordered structure can be obtained and it is possible to simulate a one-component layer either in the outermost or inner layers.

We employed GGA-PBE Hartwigsen-Goedecker-Hutter (HGH) [30] relativistic norm-conserving pseudopotentials including spin-orbit coupling (SOC). For bulk calculations, a $7 \times 7 \times 7$ mesh of k points was used for Brillouin zone integration. The atomic positions and lattice parameters were obtained during a relaxation procedure until forces became less than 10^{-5} eV/Å. To investigate the surface electronic structure, we used a supercell technique in which thin films with thickness of six to nine SLs are separated by vacuum interval of 12 Å. The k-point mesh of $7 \times 7 \times 1$ was used for the electronic structure calculations of surface.

The experiments were carried out at Helmholtz-Zentrum Berlin (BESSY II) at beamlines UE112-SGM, U125/2-SGM and at MAX-lab at I3 beamline with linearly polarized light using Scienta R4000 energy analyzer and Mott spin detector operated at 26 keV. The angle of light incidence on the sample under normal emission was 45° relative to the surface normal. The ARPES spectra were measured at various photon energies. According to the dependence of the electron mean free path, the minimal depth of probing in PES corresponds to the kinetic energy of approximately 40–100 eV. At the kinetic energies of 10–30 eV, the mean free path increases, which allows us to study the deeper layers.

The n-doping samples with stoichiometries of $PbBi_2Te_2Se_2$ and $PbBi_2Te_{1.4}Se_{2.6}$ were grown from Pb, Bi, Te, and Se powders by a modified vertical Bridgman method. Before measurements, the samples were cleaved *in situ* at room temperature in ultrahigh vacuum. The base pressure in the
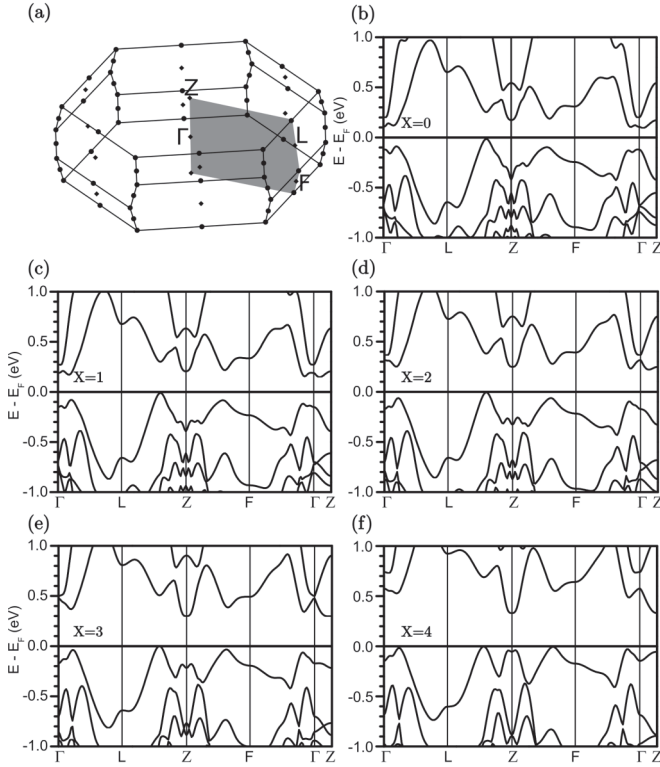
FIG. 2. (a) 3D Brillouin zone for rhombohedral elementary cell; [(b)–(f)] bulk electronic spectra of the disordered $PbBi_2Te_{4-x}Se_x$ alloy at various x.

experimental chamber during the experiment was of 1–2×10^{-10} mbar.

III. RESULTS AND DISCUSSION

A. Theoretical analysis of electronic and spin structure of disordered $PbBi_2Te_{4-x}Se_x$ alloys

According to the calculations of the bulk electronic structure of disordered $PbBi_2Te_{4-x}Se_x$ at chosen x (Fig. 2), extrema of valence and conduction bands that form the indirect band gap are located along the $L-Z$ and $\Gamma-Z$ directions, respectively. Increasing the ratio x, i.e., concentration of the Se atoms, leads to significant change of the spectra, especially in the $\Gamma-Z$ direction. Moreover, it is shown that the magnitude of the theoretical band gap increases from 90 meV ($PbBi_2Te_4$) to 303 meV ($PbBi_2Se_4$) [Fig. 3(a)]. This dependence of the band gap value on the Se concentration is linear until $x = 3$, reaching the maximum at $x = 3.5$ (309 meV). Indeed, since the Se atoms demonstrate higher electronegativity, the ionicity of the Bi-chalcogen atom bond enhances, thus resulting in the increase of the band gap. Additionally, the substitution of Te by Se leads to the decrease of the lattice parameter as well as SOC strength due to smaller ionic radius and atomic number of Se, respectively. However, within $PbBi_2Te_{4-x}Se_x$ series the band gap rises monotonously and no topological phase transition occurs.

Experimentally evaluated band gap in $PbBi_2Te_4$ is of 230 meV [7], which is more than twice as large as the theoretical one. Hence, one can expect that a series of $PbBi_2Te_{4-x}Se_x$
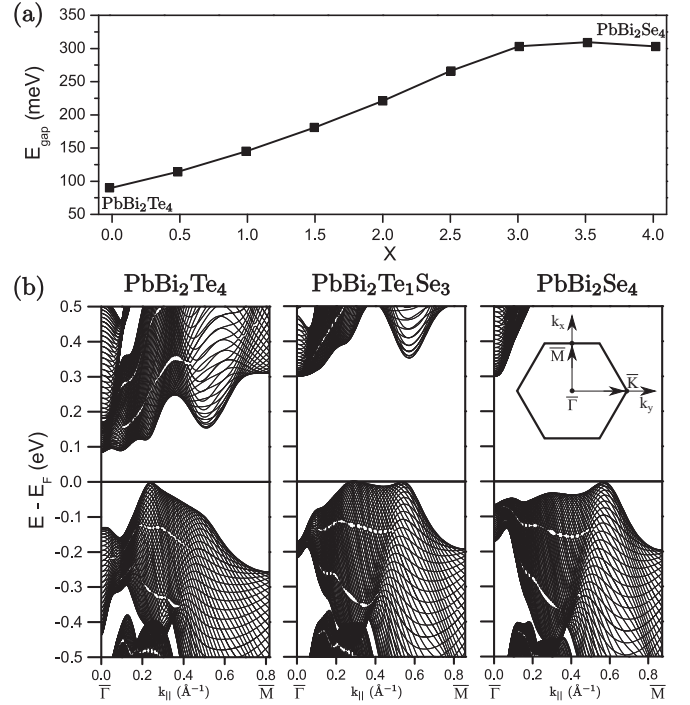

FIG. 3. (a) Dependence of band-gap value on stoichiometry and (b) evolution of the bulk band maxima in $PbBi_2Te_{4-x}Se_x$ alloy. The inset shows the high-symmetry points of the surface Brillouin zone.

compounds at high Se content may offer a large band gap. In particular, it was shown by means of optical spectroscopy and thermopower measurements that ultrathin three- to five-SL $PbBi_2Se_4$ exhibits a band gap of $\sim$600 meV [25].

In full range of x ($0 < x < 4$), these compounds are TIs, possessing bulk band gap and spin-polarized conducting surface states with linear dispersion (Fig. 4). On top of that, it is also important to identify the significant features of such electronic structure. First, increasing x leads to the shift of the Dirac point to higher energies and at $x = 4$ it is above the valence band maximum ($E_{DP} = 17$ meV). It is seen from Fig. 4(f) that the slope of the Dirac state gradually increases, so that the raise of the group velocity occurs. In turn, the aforementioned valence band maximum steadily moves along the $\bar{\Gamma}-\bar{M}$ direction away from $\bar{\Gamma}$ until $x = 3$ [Fig. 3(b)], whereas for higher x this shift abruptly increases from 0.29 Å^{-1} to 0.53 Å^{-1}, where another dominating maximum appears.

Spatial charge density distribution of the Dirac state is shown in Fig. 5. In the case $x = 0$ ($PbBi_2Te_4$), the surface state is localized within more than three SLs, and therefore a hybridization gap at the Dirac point opens in thin films of six-SL thickness. With increased Se content, the depth of propagation of the surface state steadily shifts close to the surface and at high x this state mainly concentrates in the outermost SL. This also explains the difference of values of the in-plane spin components at various x, shown in Fig. 4.

B. Theoretical and experimental study of electronic and spin structure of $PbBi_2Te_2Se_2$ and $PbBi_2Te_{1.4}Se_{2.6}$

To address the effect of the Se disordering within the Te/Se sublattice on the bulk and surface electronic structure, we performed detailed theoretical analysis of $PbBi_2Te_2Se_2$ along

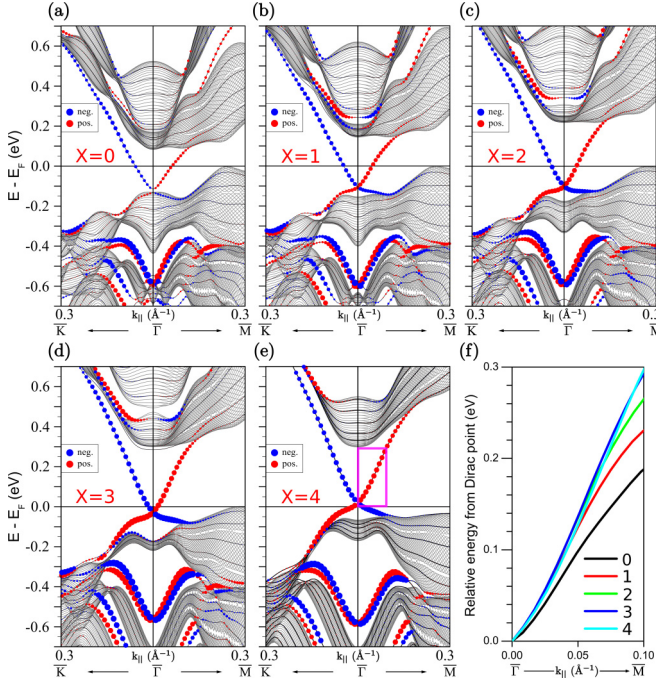FIG. 4. [(a)–(e)] Surface electronic structure of $PbBi_2Te_{4-x}Se_x$ along $\bar{K}-\bar{\Gamma}-\bar{M}$ at various x. Circles represent weights of the states, localized in the outermost SL, multiplied by value of in-plane spin components (red and blue colors denote positive and negative values of spin, respectively). (f) Superimposed Dirac-cone states in the $\bar{\Gamma}-\bar{M}$ direction; the region under consideration is shown on panel (e).

with experimental study. There exist two possible configurations of crystal structure of the ordered $PbBi_2Te_2Se_2$ compound. In these configurations, atomic layers are stacked along the (111) direction in the following sequences [Figs. 1(c) and 1(d)]: Se-Bi-Te-Pb-Te-Bi-Se ("configuration I") and Te-Bi-Se-Pb-Se-Bi-Te ("configuration II"). According to Vegard's law as well as experimentally measured parameters [22,23,27] for these cases, we set the lattice parameters as $a = 4.2995$ Å and $c = 40.4385$ Å and performed optimization of atomic positions.
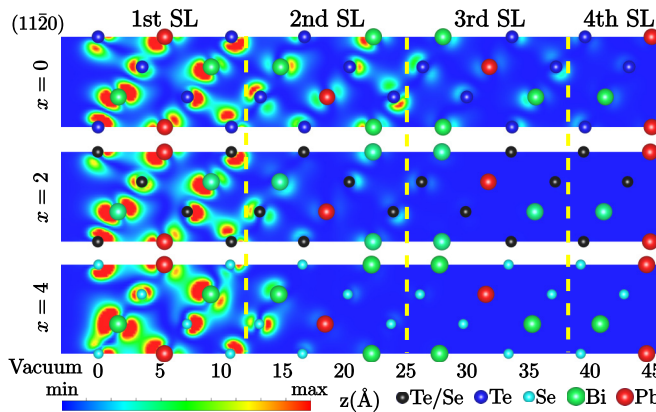

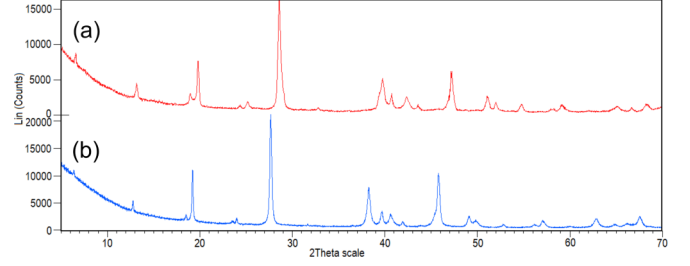FIG. 5. Spatial charge density distribution of the Dirac state at $x = 0, 2, 4$.

FIG. 6. XRD patterns for $PbBi_2Te_2Se_2$ ($x = 2.0$) (a) and $PbBi_2Te_4$ ($x = 0$) (b) from a powder of single crystals.

The synthesized crystals ($x = 2.0$ and 2.6) were characterized by powder x-ray diffraction using a Bruker D8 ADVANCE diffractometer with Cu-Kα radiation. The obtained pattern for the ordered $x = 2.0$ phase is presented in Fig. 6(a). Apparently, it is just a single phase without a trace of impurities or a signature of other phases and displays the diffraction lines which are qualitatively similar to those in rhombohedral R$\bar{3}$m crystal structure of the $PbBi_2Te_4$ compound [Fig. 6(b)]. Comparing to the x-ray diffraction (XRD) pattern of the $PbBi_2Te_4$ phase, the peak positions for the $PbBi_2Te_2Se_2$ compound are shifted toward higher angles due to Se_{Te} substitution in the crystal lattice.

Calculated spectra (Fig. 7) show that the ordered $PbBi_2Te_2Se_2$ compounds also exhibit semiconductor-like behavior in the bulk; however, depending on the Te/Se layers content, the band gap significantly changes. Among three cases, including the disordered structure, "configuration II" with Te atoms in the outermost layers has the largest band gap (278 meV), whereas "configuration I" has the smallest one (90 meV). Inducing the disordering of the crystal structure does not affect the position of the top of the valence band. As for the surface states, in "configuration I" the Dirac point is located close to the valence band maximum energy, while in other cases it is lower by more than 60 meV. Next, it is seen that in the vicinity of $\bar{\Gamma}$ the cone is significantly narrower and the conduction band bottom lies quite close to the Fermi level. Besides, group velocity exceeds almost twice the corresponding values for other two cases. As for the charge density distribution, the Dirac state at the $\bar{\Gamma}$ point is located within 2 SLs as depicted in Fig. 5 for $x = 2$.

ARPES spectra of the $PbBi_2Te_2Se_2$ sample are shown in Fig. 8(a) (left column) at various photon energies. One can clearly see the Dirac cone with the Dirac point located at binding energy of $\sim$0.6 eV, especially for photon energy $h\nu = 60$ eV. In accordance with previous studies [31–33], the state dispersing from 0.3 eV at the $\bar{\Gamma}$ point to the Fermi level at higher k is the two-dimensional electron gas (2DEG) state, formed due to the band bending at the surface. The state, located directly at the Fermi level, is related to the conduction band (see panels $h\nu = 25$ eV) [10]. The behavior of these electron states can also be seen in the isoenergy cuts of the spectra, shown in Fig. 8(b). It is seen that increasing of the photon energy enhances the intensity of the Dirac cone relative to the bulk bands, confirming the surface localization of the topological surface state.

To capture the effect of the stoichiometry on the electronic structure, we have measured ARPES spectra of the sample
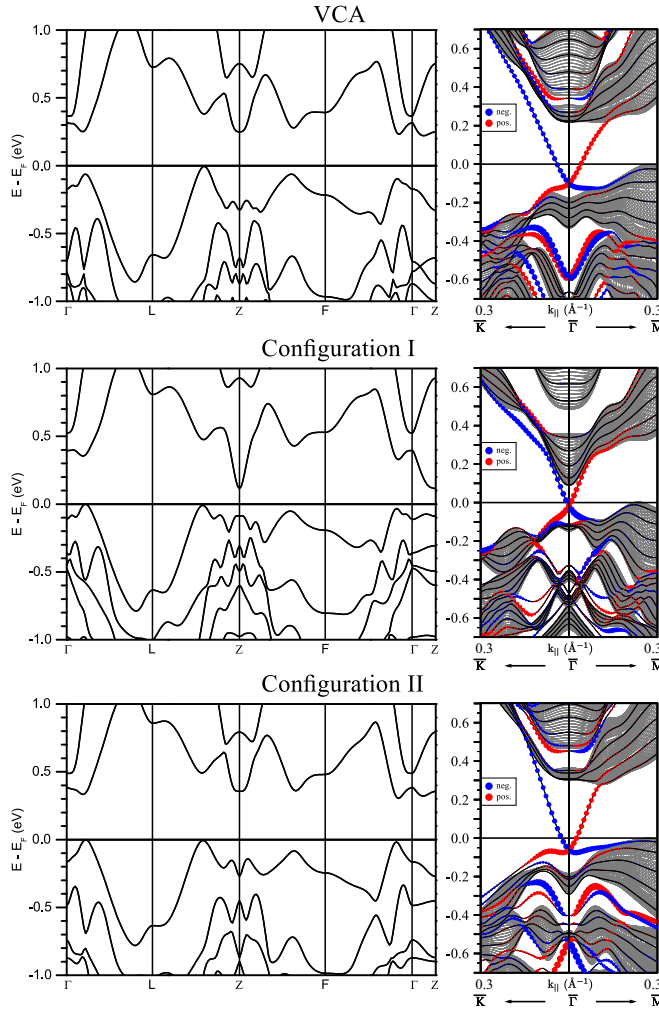
FIG. 7. (Left) bulk electronic spectra and (right) surface electronic spectra of three configurations of $PbBi_2Te_2Se_2$. Circles represent weights of the states, localized in the outermost SL, multiplied by value of in-plane spin components (red and blue colors denote positive and negative values of spin, respectively).

FIG. 8. (a) ARPES spectra of $PbBi_2Te_2Se_2$ (left column) and $PbBi_2Te_{1.4}Se_{2.6}$ (right column) samples measured in the $\bar{K}-\bar{\Gamma}-\bar{K}$ direction at various photon energies. (b) Full 3D mapping of the dispersion relations in k space and (c) spin-resolved ARPES spectra taken for two emission angles, corresponding to the wave vectors of -0.1 $\mathring{A}^{-1}$ and 0.1 $\mathring{A}^{-1}$, for $PbBi_2Te_2Se_2$ measured at 25-eV photon energy.

$PbBi_2Te_{1.4}Se_{2.6}$, shown in Fig. 8(a) (right column). It is seen that the Dirac point in this case is located at binding energy of 0.5 eV. The difference of ~ 100 meV in the Dirac point position between $PbBi_2Te_2Se_2$ and $PbBi_2Te_{1.4}Se_{2.6}$ can be explained by the different position of the Fermi level for two samples, similar to results of Ref. [12]. The measured group velocities (the Dirac-cone slopes) near the Dirac point are nearly identical for these two samples.

In order to investigate the spin structure of $PbBi_2Te_2Se_2$ we have carried out the spin-ARPES measurements with using the Mott detector. From Fig. 8(c), one can clearly see that the upper branches of the topological surface states are spin polarized with the quantization axis perpendicular to the momentum. The spin polarization of the lower branches of the Dirac cone is less pronounced due to mixing with the valence band states.

The calculated Dirac-cone dispersions along the $\bar{K}-\bar{\Gamma}-\bar{M}$ direction for $PbBi_2Te_2Se_2$, superimposed on the experimental ARPES results, are shown in Fig. 9. Here, the binding energy of the calculated Dirac point is aligned with respect to the
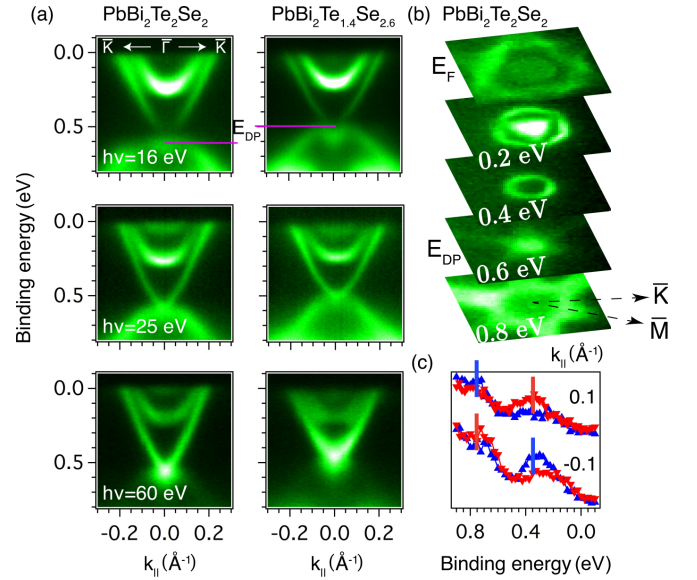
experimental one. Comparison of dispersions reveals that in the disordered alloy obtained from VCA method the valence band in the $\bar{\Gamma}-\bar{K}$ direction as well as the slopes of the Dirac cone in both directions are in a good agreement with experiment. However, the conduction band is not correctly reproduced. In the case of "configuration II", the calculated cone is slightly narrower but the bulk states coincide better. As for "configuration I", the experimental and theoretical spectra are remarkably different. The same analysis has been done for $PbBi_2Te_{1.4}Se_{2.6}$ compound and it was found that it shows a similar tendency. From this, one can conclude that in terms of employed approach "configuration II", when the outermost atomic layers of SL are occupied by Te, is in better agreement with the experimental data.
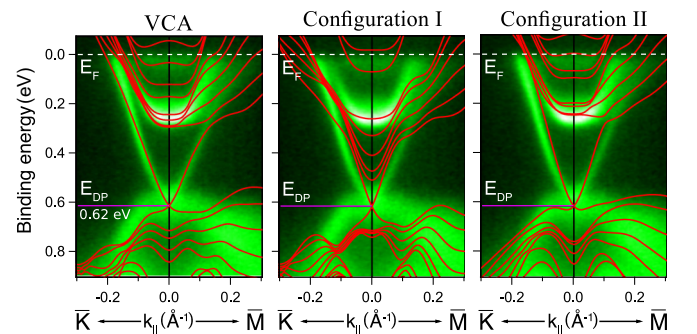

FIG. 9. ARPES measurement at 25-eV photon energy on $PbBi_2Te_2Se_2$ with overlaid surface band structure obtained from DFT calculations (red lines).

IV. CONCLUSION

In conclusion, we have presented a systematic investigation of the electronic and spin structure of a series of topological insulators $PbBi_2Te_{4-x}Se_x$. It was found that increasing Se content leads to the increase of the band gap in theory up to 300 meV, which is three times larger than the value of the starting $PbBi_2Te_4$ compound. Variation of composition significantly affects the electronic surface structure. The position of the Dirac point shifts closer to the Fermi level and the Dirac cone becomes more pronounced; also the group velocity of charge carriers increases. Using spin- and angle-resolved photoemission spectroscopy, it was shown that the $PbBi_2Te_2Se_2$ and $PbBi_2Te_{1.4}Se_{2.6}$ compounds are characterized by well-defined spin-polarized topological surface state in the bulk gap. DFT calculations better reproduce photoemission data when all Te atoms are concentrated in the outermost layers of SL. However, even some mixing of Se and Te gives quite good agreement with the experiment.

[1] A. Bansil, H. Lin, and T. Das, Rev. of Mod. Phys. **88**, 021004 (2016).

[2] Y. Ando, J. Phys. Soc. Jpn. **82**, 102001 (2013).

[3] Y. L. Chen, J. G. Analytis, J.-H. Chu, Z. K. Liu, S.- K. Mo, X. L. Qi, H. J. Zhang, D. H. Lu, X. Dai, Z. Fang, S. C. Zhang, I. R. Fisher, Z. Hussain, and Z.-X. Shen, Science **325**, 178 (2009).

[4] Y. Xia, D. Qian, D. Hsieh, L. Wray, A. Pal, H. Lin, A. Bansil, D. Grauer, Y. S. Hor, R. J. Cava, and M. Z. Hasan, Nat. Phys. **5**, 398 (2009).

[5] S. Kim, M. Ye, K. Kuroda, Y. Yamada, E. E. Krasovskii, E. V. Chulkov, K. Miyamoto, M. Nakatake, T. Okuda, Y. Ueda, K. Shimada, H. Namatame, M. Taniguchi, and A. Kimura, Phys. Rev. Lett. **107**, 056803 (2011).

[6] I. V. Silkin, T. V. Menshchikova, M. M. Otrokov, S. V. Eremeev, Yu M. Koroteev, M. G. Vergniory, V. M. Kuznetsov, and E. V. Chulkov, JETP Lett. **96**, 322 (2012).

[7] K. Kuroda, H. Miyahara, M. Ye, S. V. Eremeev, Yu. M. Koroteev, E. E. Krasovskii, E. V. Chulkov, S. Hiramoto, C. Moriyoshi, Y. Kuroiwa, K. Miyamoto, T. Okuda, M. Arita, K. Shimada, H. Namatame, M. Taniguchi, Y. Ueda, and A. Kimura, Phys. Rev. Lett. **108**, 206803 (2012).

[8] T. Okuda, T. Maegawa, M. Ye, K. Shirai, T. Warashina, K. Miyamoto, K. Kuroda, M. Arita, Z. S. Aliev, I. R. Amiraslanov, M. B. Babanly, E. V. Chulkov, S. V. Eremeev, A. Kimura, H. Namatame, and M. Taniguchi, Phys. Rev. Lett. **111**, 206803 (2013).

[9] S. V. Eremeev, G. Landolt, T. V. Menshchikova, B. Slomski, Yu. M. Koroteev, Z. S. Aliev, M. B. Babanly, J. Henk, A. Ernst, L. Patthey, A. Eich, A. Ako Khajetoorians, J. Hagemeister, O. Pietzsch, J. Wiebe, R. Wiesendanger, P. M. Echenique, S. S. Tsirkin, I. R. Amiraslanov, J. H. Dil, and E. V. Chulkov, Nat. Commun. **3**, 635 (2012).

[10] T. Arakane, T. Sato, S. Souma, K. Kosaka, K. Nakayama, M. Komatsu, T. Takahashi, Z. Ren, K. Segawa, and Y. Ando, Nat. Commun. **3**, 636 (2012).

[11] S. Muff, F. von Rohr, G. Landolt, B. Slomski, A. Schilling, R. J. Cava, J. Osterwalder, and J. H. Dil, Phys. Rev. B **88**, 035407 (2013).

[12] A. M. Shikin, I. I. Klimovskikh, S. V. Eremeev, A. A. Rybkina, M. V. Rusinova, A. G. Rybkin, E. V. Zhizhin, J. Sánchez-Barriga, A. Varykhalov, I. P. Rusinov, E. V. Chulkov, K. A. Kokh, V. A. Golyashov, V. Kamyshlov, and O. E. Tereshchenko, Phys. Rev. B **89**, 125416 (2014).

[13] I. I. Klimovskikh, D. Sostina, A. Petukhov, A. G. Rybkin, S. V. Eremeev, E. V. Chulkov, O. E. Tereshchenko, K. A. Kokh, and A. M. Shikin, Sci. Rep. **7**, 45797 (2017).

[14] Z. Ren, A. A. Taskin, S. Sasaki, K. Segawa, and Y. Ando, Phys. Rev. B **82**, 241306(R) (2010).

[15] W. Ko, I. Jeon, H. W. Kim, H. Kwon, S.-J. Kahng, J. Park, J. S. Kim, S. W. Hwang, and H. Suh, Sci. Rep. **3**, 2656 (2013).

[16] S. Souma, K. Eto, M. Nomura, K. Nakayama, T. Sato, T. Takahashi, K. Segawa, and Y. Ando, Phys. Rev. Lett. **108**, 116801 (2012).

[17] M. Neupane, S.-Y. Xu, L. A. Wray, A. Petersen, R. Shankar, N. Alidoust, Ch. Liu, A. Fedorov, H. Ji, J. M. Allred, Y. S. Hor, T.-R. Chang, H.-T. Jeng, H. Lin, A. Bansil, R. J. Cava, and M. Z. Hasan, Phys. Rev. B **85**, 235406 (2012).

[18] G. Hao, X. Qi, L. Xue, C. Cai, J. Li, X. Wei, and J. Zhong, J. Appl. Phys. **113**, 024306 (2013)

[19] L. E. Shelimova, O. G. Karpinskii, T. E. Svechnikova, E. S. Avilov, M. A. Kretova, and V. S. Zemskov, Inorg. Mater. **40**, 1264 (2004).

[20] M. G. Kanatzidis, Acc. Chem. Res. **38**, 359 (2005).

[21] K. Nakayama, K. Eto, Y. Tanaka, T. Sato, S. Souma, T. Takahashi, K. Segawa, and Y. Ando, Phys. Rev. Lett. **109**, 236804 (2012).

[22] H. Liu and L. Y. Chang, Am. Mineral. **79**, 1159 (1994).

[23] K. A. Agaev and S. A. Semiletov, Kristallografiya **13**(2), 258 (1968).

[24] H. Jin, J.-H. Song, A. J. Freeman, and M. G. Kanatzidis, Phys. Rev. B **83**, 041202(R) (2011).

[25] A. Chatterjee, S. N. Guin, and K. Biswas, Phys. Chem. Chem. Phys. **16**, 14635 (2014).

[26] L. Zhang and D. J. Singh, Phys. Rev. B **81**, 245119 (2010).

[27] L. A. Kuznetsova, V. L. Kuznetsov, and D. M. Rowe, J. Phys. Chem. Solids **61**, 1269 (2000).

[28] X. Gonze, B. Amadon, P.-M. Anglade, J.-M. Beuken, F. Bottin, P. Boulanger, F. Bruneval, D. Caliste, R. Caracas, M. Cote, T. Deutsch, L. Genovese, Ph. Ghosez, M. Giantomassi, S. Goedecker, D. R. Hamann, P. Hermet, F. Jollet, G. Jomard, S. Leroux, M. Mancini, S. Mazevet, M. J. T. Oliveira, G. Onida, Y. Pouillon, T. Rangel, G.-M. Rignanese, D. Sangalli, R. Shaltaf, M. Torrent, M. J. Verstraete, G. Zerah, and J. W. Zwanziger, Comput. Phys. Commun. **180**, 2582 (2009); [http://www.abinit.org]

[29] A. R. Denton and N. W. Ashcroft, Phys. Rev. A **43**, 3161 (1991).

[30] C. Hartwigsen, S. Goedecker, and J. Hutter, Phys. Rev. B **58**, 3641 (1998).

[31] M. S. Bahramy, P. D. C. King, A. de la Torre, J. Chang, M. Shi, L. Patthey, G. Balakrishnan, P. Hofmann, R. Arita, N. Nagaosa, and F. Baumberger, Nat. Commun. **3**, 1159 (2012).

[32] M. Bianchi, R. C. Hatch, J. Mi, B. B. Iversen, and P. Hofmann, Phys. Rev. Lett. **107**, 086802 (2011).

[33] S. V. Eremeev, M. G. Vergniory, T. V. Menshchikova, A. A. Shaposhnikov, and E. V. Chulkov, New J. Phys. **14**, 113030 (2012).